

Wavelet based system identification for a nonlinear experimental model

Luyu Li^{*1,2}, Han Qin² and Yun Niu²

¹State Key Laboratory of Coastal and Offshore Engineering, Dalian University of Technology, Dalian, Liaoning, China, 116024

²School of Civil Engineering, Dalian University of Technology, Dalian, Liaoning, China, 116024

(Received October 13, 2016, Revised September 17, 2017, Accepted September 18, 2017)

Abstract. Traditional experimental verification for nonlinear system identification often faces the problem of experiment model repeatability. In our research, a steel frame experimental model is developed to imitate the behavior of a single story steel frame under horizontal excitation. Two adjustable rotational dampers are used to simulate the plastic hinge effect of the damaged beam-column joint. This model is suggested as a benchmark model for nonlinear dynamics study. Since the nonlinear form provided by the damper is unknown, a Morlet wavelet based method is introduced to identify the mathematical model of this structure under different damping cases. After the model identification, earthquake excitation tests are carried out to verify the generality of the identified model. The results show the extensive applicability and effectiveness of the identification method.

Keywords: nonlinear system identification; wavelet transform; nonlinear test model; adjustable dampers; shake table test

1. Introduction

Research considering verification of nonlinear system identification methods mainly relies on numerical simulation. Few researchers have conducted physical experiment. Nonlinearities presented in buildings are often caused by damages, and the damaging tests are very expensive for study in civil engineering. Due to the uncertainty contained in material, test environment and construction process, the behavior of the experimental model in different tests is unrepeatability.

To solve this problem, many researchers have proved the effectiveness of identification methods by conducting geometrical nonlinearity model test. Geometrical nonlinearity is often caused by large deformation. Noël and Kerschen (2013) made a device that consists of two cantilever beams, a thick one and a much thinner one, with both of their free end solidly connected inline, to provide geometrical nonlinearity. There are also researchers like Aykan and Nevzat Özgüven (2013) and Magnevall *et al.* (2012) who have implemented similar methods to realize geometrical nonlinearity.

However, in civil engineering, material nonlinearity is usually the main cause of structural nonlinearity. There are full scale tests, Moaveni and Asgariéh (2012) built a seven-story shear wall structure to study its nonlinear behavior under earthquake excitation; Asgariéh *et al.* (2014) constructed a large scale three-story reinforced concrete frame with masonry infill. These two buildings are both expensive. On account of this, scale model or component test is also a reasonable choice. Kitada (1998) designed a scale five-story steel model. The fifth story of this model is

much weaker than the rest to reduce the effort required for the top story to yield. The experiments introduced tests are all one-off test, reproducing of the test data is statistically unrealistic.

Material nonlinearity could cause unrecoverable damages such as yielding in steel members, crack and crush in concrete components, etc. Therefore, instead of steel and concrete, Ma *et al.* (2006) made twenty T-shape wooden specimens. Each specimen consisted of two laminated veneer lumber members connected with plywood gusset plates. Wood presents similar hysteresis constitution as steel and concrete do but costs less. Ortiz *et al.* (2013) made cheaper ferrocement walls. These experiments costed less, but still have the repeatability problem. Some studies have already focused on realizing nonlinearity without material damage. Zhou *et al.* (2008) came up with the idea of relying on a hydraulic cylinder-piston system to simulate sudden change of stiffness in structures. Ta and Lardiès (2006) devised an open-loop control system to force a cantilever beam to behave similarly like a single degree of freedom (SDOF) system with nonlinear stiffness and nonlinear viscous damping. In this paper, an experimental model is introduced in section 2, that could simulate more complex structures.

Nonlinear system identification method have been developing rapidly in the recent half century. Some methods assume that the model of the structure is known before hand, such as reverse path method introduced by Rice and Fitzpatrick (1988) and nonlinear as feed-back method by Adams and Allemang (2000), etc. Some methods do not require the model of the structure. They use a universal model to approximate every physical model, for instance, Haber and Unbehauen (2010) adopted the NARMAX method in nonlinear system identification, Amari (1998) utilized the nonlinear neural network method to imitate the behavior of unknown nonlinear system. Methods based on

*Corresponding author, Professor
E-mail: liluyu@yeah.net

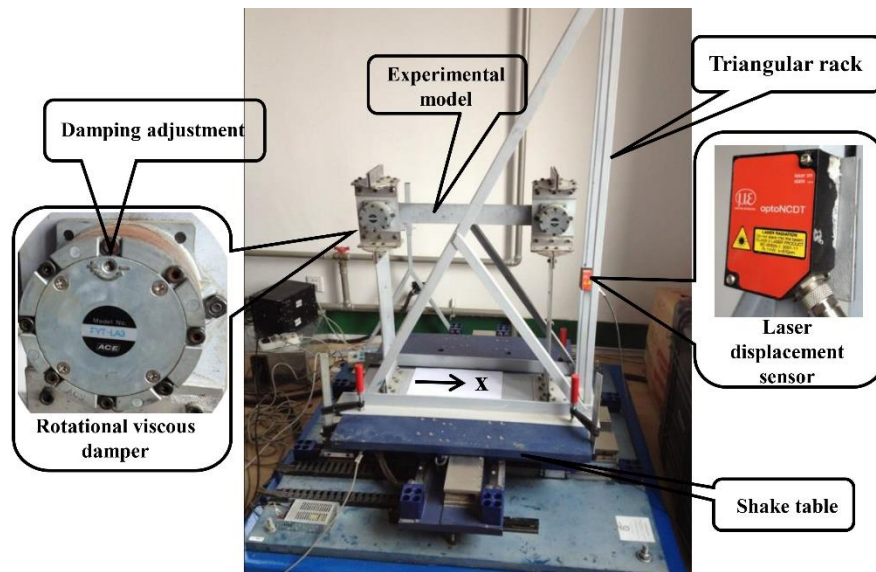


Fig. 1 Structural nonlinear vibration model

wavelet transform have been attracting much attention in civil engineering for years. Because it requires little knowledge about the structure, while visually presents the relationship between the model and the time-frequency variables.

The application of wavelet transform for system identification has developed from linear to nonlinear, from simple model to more complex model. For linear system identification, Le and Paultre (2012) extend the use of the continuous wavelet transform (CWT) identification method to ambient excited linear structure. Some researchers have identified nonlinear system as linear time varying system. Shi *et al.* (2006) identified the linear time-varying parameters of a chain like structure with wavelet and least square method. Some studies have directly identified parameters of nonlinear system. Staszewski (1998) identified nonlinear damping and stiffness by extracting the wavelet ridge of the Morlet wavelet transformation and fit the extracted envelop and backbone curve with the formula obtain by perturbation method. In this method, nonlinear form of the structure should be known beforehand. Ta and Lardiès (2006) improved this method to identify nonlinear characteristics (damping and stiffness) without prior knowledge about the structure nonlinearity. Other improvements have focused on different details of the identification method. Dai *et al.* (2009) recommended a new algorithm for ridge detection to eliminate the frequency-shift effect of the wavelet ridge. Wang *et al.* (2009) conducted singular value decomposition on the time-frequency spectrum matrix to reduce the influence of noise when extracting the wavelet ridge. Articles written by Like Boltežar and Slavič (2004), Kijewski and A (2003), Slavič and Boltežar (2011) and Yi *et al.* (2006) have focused on tackling the edge effect caused by wavelet transformation.

In this research, a single story steel frame with two adjustable rotational viscous dampers was designed to realize nonlinear behaviors. The rotational viscous dampers

were used to imitate the plastic hinge effect of frame structures. With this device, costly and damaging physical experiment for identification method verification could be avoided. This device is capable of offering stable and repeatable response for online and offline identification. By adjusting the damper, different levels of nonlinearity can be obtained. This model is also suitable for nonlinear dynamics study, nonlinear structural control method, etc.

Since the nonlinear form of the damper is unknown, it is a great challenge for an identification method to simultaneously estimate the form of nonlinearity and evaluate the parameters. In our research, an identification method based on the Morlet wavelet transform is introduced to solve this problem.

The physical and mathematical model are studied in section 2. In section 3 and section 4, a brief introduction of the CWT theory and the procedure of the identification method are presented. In section 5, this method is implemented with the data acquired from the free vibration of the structure in the cases of different damping scale. The efficiency of this identified method is verified through earthquake tests.

2. Description and mathematical modeling of the experimental model

2.1 Experimental setups of the structural model

The experimental model is a single story steel frame. It was designed to simulate the nonlinear behavior of a single story steel frame structure. The components of the steel frame are as follows, two 500 mm×150 mm×3 mm 25Mn steel plates function as the columns, a 500 mm×50 mm×5 mm steel bar as the beam. These three components are connected with two rotational viscous dampers by

accessories. With each damper 2.3 Kg, the distance between the axis of the damper and the 25Mn steel plate is 10 cm. It is well known in practice that, under large horizontal load, such as earthquake or strong wind, the beam-column joint of steel frame is often damaged. This introduces plastic hinge effect into the structure. The dampers were assembled at the position of beam-column joint to imitate the effect of a plastic hinge. As is depicted in Fig. 1, the components of the frame are assembled in such a way that the frame can be regarded as an SDOF system. The frame was firmly mounted on the shake table.

The rotational viscous damper is adjustable. There is a screw with a mark ‘+ -’ around it, as is shown in the partial enlarged figure to the left of Fig. 1. By switching this screw, we can increase or decrease the viscous damping. Different damage levels can be simulated by adjusting the viscous damper. In this research, we specify three conditions to the damper, namely large damping case, small damping case and medium damping case, corresponding to the screw position in the clockwise end, counter clockwise end, in the middle between both ends.

In Fig. 1, the triangular rack was mounted on the shake table to fix the laser displacement sensor. This rack should be sufficiently stiff to ensure the collected data couldn't be interfered by the vibration of the rack. The laser displacement sensor is produced by Micro-Epsilon. A signal acquisition device produced by the National Instrument was used to acquire the signal output from the sensor. The displacements in this experiment were recorded with a sampling frequency of 1000 Hz. The shake table and its control system is produced by Quanser.

2.2 Analysis of the experimental model

Assume that the structure moves horizontally and neglect the frictions involve in the connections and the rotating of the damper. Moreover, due to the large bending stiffness difference between the steel columns and other parts of the frame in the x - y plane, except for the steel plate, the rest part of the frame can be regarded as rigid bodies. Then the physical model can be simplified as is illustrated in Fig. 2. In Fig. 2, two identical cantilever columns, which consist of an elastic part of length l and a rigid part of length l_1 , are connected with a rectangular rigid beam through two round axles. The rigid beam couples the translational degree of freedoms of the column tips; and the two axles offer resistance against the rotation of the column tips. Since these two columns are identical and connected in parallel, it can be considered as a single thicker cantilever beam with a rigid part on the top, as illustrated in Fig. 3.

The direction of the forces and displacement are illustrated in Fig. 3. As is shown in this diagram at the tip of the beam, the resistance moment M is the resultant of damping moment. The equivalent force F in x direction is the combination of inertia force and equivalent damping force generated in the steel columns. Since the form of the resistance moment M is unknown, we use $g(\theta_e, \dot{\theta}_e)$ to represent the relationship between M and the tip angle θ_e and its rotational velocity $\dot{\theta}_e$.

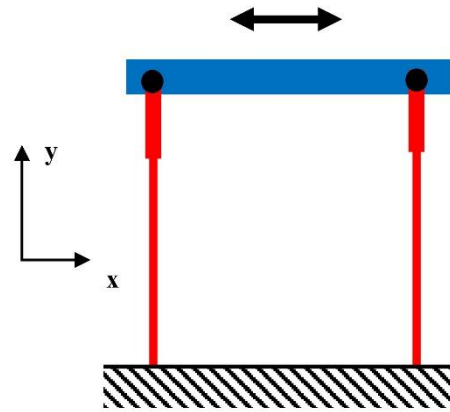


Fig. 2 Simplified model of the test frame

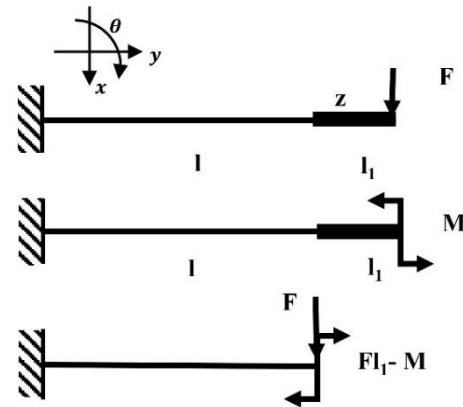


Fig. 3 Calculation model of the test frame

$$P_m = M_{in} M_{ex} P_w \quad (1)$$

$$F = -m\ddot{x}_e - c\dot{x}_e \quad (2)$$

An assumption of small deformation theory is used in the derivation of the equation of motion (EOM). The inertia of the steel beam as well as the inertia in y direction and rotation is omitted.

Firstly, the geometrical and physical relationships between the free end and elastic end is derived, which is marked by the subscript e and z respectively. x_e and θ_e (resp. x_z and θ_z) respectively stands for the displacement in x direction and the rotation angle of the free end (resp. elastic end.). F_z and M_z represent the equivalent force applied on the elastic end.

$$\theta_e = \theta_z \quad (3)$$

$$x_e = x_z + \theta_z l_1 \quad (4)$$

$$F_z = F \quad (5)$$

$$M_z = Fl_1 - M \quad (6)$$

The rotational and translational displacement of the tip can be found in Mechanics of Materials written by Gere and Timoshenko (1991). The relationships between displacement and force of the structure are derived as follows. In the following equations, E stands for Young's modulus of the steel plate, I stands for the moment of inertia of the cross section.

To obtain the displacement of the elastic end with respect to the free end force, it can be derived

$$\begin{aligned} \theta_z &= \frac{F_z l^2}{2EI} + \frac{M_z l}{EI} = \frac{Fl^2}{2EI} + \frac{Fl_1 - M}{EI} \\ &= \frac{F(l^2 + 2ll_1)}{2EI} - \frac{Ml}{EI} \end{aligned} \quad (7)$$

$$\begin{aligned} x_z &= \frac{F_z l^3}{3EI} + \frac{M_z l^2}{2EI} = \frac{Fl^3}{3EI} + \frac{Fl^2 l_1 - Ml^2}{2EI} \\ &= \frac{F(2l^3 + 3l^2 l_1)}{6EI} - \frac{Ml^2}{2EI} \end{aligned} \quad (8)$$

Substituting (7), (8) to (3) and (4) gives

$$\theta_e = \frac{F(l^2 + 2ll_1)}{2EI} - \frac{Ml}{EI} \quad (9)$$

$$\begin{aligned} x_e &= \frac{F(2l^3 + 3l^2 l_1)}{6EI} - \frac{Ml^2}{2EI} + \left[\frac{F(l^2 + 2ll_1)}{2EI} - \frac{Ml}{EI} \right] l_1 \\ &= \frac{F(2l^3 + 6l^2 l_1 + 6ll_1^2)}{6EI} - \frac{M(l^2 + 2ll_1)}{2EI} \end{aligned} \quad (10)$$

Through the rearrangement of Eqs. (9) and (10), Eqs. (11) and (12) can be obtained.

$$\theta_e = \frac{l^2 + 2ll_1}{2EI} F - \frac{l}{EI} M \quad (11)$$

$$x_e = \frac{2l^3 + 6l^2 l_1 + 6ll_1^2}{6EI} F - \frac{l^2 + 2ll_1}{2EI} M \quad (12)$$

Solving this equations, we get F and M with respect to θ_e and x_e .

$$\begin{aligned} F &= \left(\frac{l^2 + 2ll_1}{2EI} \theta_e - \frac{l}{EI} x_e \right) \times \frac{12E^2 I^2}{l^4} \\ &= -\frac{6(l + 2l_1)EI}{l^3} \theta_e + \frac{12EI}{l^3} x_e \end{aligned} \quad (13)$$

$$\begin{aligned} M &= \left(\frac{2l^3 + 6l^2 l_1 + 6ll_1^2}{6EI} \theta_e - \frac{l^2 + 2ll_1}{2EI} x_e \right) \times \frac{12E^2 I^2}{l^4} \\ &= -\frac{4(l^2 + 3ll_1 + 3l_1^2)EI}{l^3} \theta_e + \frac{6(l + 2l_1)EI}{l^3} x_e \end{aligned} \quad (14)$$

Substituting (1), (2), into (13) and (14) gives

$$m\ddot{x}_e + c\dot{x}_e + \frac{12EI}{l^3} x_e - \frac{6(l + 2l_1)EI}{l^3} \theta_e = 0 \quad (15)$$

$$g(\theta_e, \dot{\theta}_e) = -\frac{4(l^2 + 3ll_1 + 3l_1^2)EI}{l^3} \theta_e + \frac{6(l + 2l_1)EI}{l^3} x_e \quad (16)$$

$g(\theta_e, \dot{\theta}_e)$ may consists of polynomial with respect to θ_e , $\dot{\theta}_e$ or other nonlinear forms. From the performance of the experiments in this research, $g(\theta_e, \dot{\theta}_e)$ is relevant to $\dot{\theta}_e$, which makes $\frac{6(l + 2l_1)EI}{l^3} \theta_e$ in (15) a nonlinear restoring force term. For example, if $g(\theta_e, \dot{\theta}_e)$ linearly relates to the angular velocity, i.e. $g(\theta_e, \dot{\theta}_e) = \xi \dot{\theta}_e$ (ξ is a constant), the damper will form another dynamic system that offer resistance against the rotation of the free end.

Since the real model of the damper $g(\theta_e, \dot{\theta}_e)$ is unknown, a nonlinear mapping with respect to x_e and \dot{x}_e is used to approximate the nonlinear response of the damper. Restrict the rotation of the damper, the first order frequency of this linear counterpart shows little difference from that of the nonlinear counterpart. The influence of nonlinearity in this structure is small relative to its linear counterpart. To simplify analysis of these weak nonlinear system, a small parameter ϵ is added before the nonlinear restoring force term. Eq. (17) can be used as a universal nonlinear term.

$$c\dot{x}_e - \frac{6(l + 2l_1)EI}{l^3} \theta_e \cong \epsilon f(x_e, \dot{x}_e) \quad (17)$$

where \cong means 'approximate by'.

The EOM of this structure is approximated by

$$\ddot{x}_e + \omega_0^2 x_e + \epsilon f(x_e, \dot{x}_e) = 0 \quad (18)$$

where

$$\omega_0^2 = \frac{12EI}{ml^3} \quad (19)$$

In section 4, it will be studied to use this EOM to imitate the behavior of the steel frame.

3. The complex Morlet wavelet transform and the ridge of scalogram

3.1 Theory of complex Morlet wavelet transform

In this section, we introduce the theory of complex

Morlet wavelet transform, details of the proof and derivation can refer to the book: a wavelet tour of signal processing by Mallat (1999). Wavelet analysis is mainly discussed in $L^2(\mathbb{R})$ space. $L^2(\mathbb{R})$ is a function space, consisting of square integrable functions defined over rational number space \mathbb{R}

$$f(t) \in L^2(\mathbb{R}) \Leftrightarrow \int_{\mathbb{R}} |f(t)|^2 dt < +\infty \quad (20)$$

In signal processing, Eq. (20) shows that $f(t)$ is an energy limited signal and $L^2(\mathbb{R})$ is called energy limited signal space. $|\bullet|$ returns the modulus of a function. In the theory of wavelet transform, we define $\psi(t)$ as the basic wavelet or mother wavelet and generally $\psi(t) \in L^2(\mathbb{R})$. Let's define the Fourier transformation of $\psi(t)$ as $\hat{\psi}(\omega)$. $\hat{\psi}(\omega)$ should satisfy the admissible condition

$$\int_{-\infty}^{+\infty} |\omega|^{-1} |\hat{\psi}(\omega)|^2 d\omega < \infty \quad (21)$$

The continuous wavelet transform of the signal $f(t)$ is defined as

$$W_{\psi,f}(a,b) = \langle f, \psi_{a,b} \rangle = \frac{1}{\sqrt{a}} \int_{-\infty}^{+\infty} f(t) \psi^*\left(\frac{t-b}{a}\right) dt \quad (22)$$

a is the scale factor and b is the shift factor, $a, b \in \mathbb{R}$. $\psi^*(t)$ is the complex conjugate of $\psi(t)$. $\langle \bullet \rangle$ calculates the inner product in $L^2(\mathbb{R})$ space. One of the most widely used wavelet is the Morlet wavelet, which is defined in the time domain as

$$\psi(t) = \frac{1}{\sqrt{\pi f_b}} e^{j2\pi f_c t} e^{-t^2/f_b} \quad (23)$$

f_b is the bandwidth parameter, and f_c is the wavelet center frequency. It is worth noting that the complex Morlet wavelet does not satisfy the admissibility condition. However, when $f_c \sqrt{f_b} \geq \sqrt{2}$, the complex Morlet wavelet approximately satisfies the admissible condition. Under this condition, it is able to serve as a wavelet as is stated by Yan *et al.* (2006). The complex Morlet wavelet is selected because of its good locality in both time and scale (frequency) domain.

There is a correspondence between the frequency f in time-frequency domain and scale a the time-scale space.

$$f = \frac{f_c}{a} f_s \quad (24)$$

where f_s is the sample frequency of the signal $f(t)$.

The complex Morlet wavelet transformation of the signal, which is called the scalogram of the signal, can be represented as follows

$$W(a,b) = \frac{\sqrt{a}}{2} A(b) e^{\frac{-f_b(a\hat{\phi}(b)-2\pi f_c)^2}{4}} e^{j\phi(b)} \quad (25)$$

3.2 The ridge of scalogram

The wavelet ridge curve is usually extracted by finding the extremum at each time point of $|W_u(a,b)|$. However, Delprat *et al.* (1992) argued that a frequency-shift phenomenon is discovered in the magnitude of the scalogram. This will affect the precision of the parameter identification. In order to eliminate the influence of this phenomenon, we adopt a method given by Dai *et al.* (2009). In this method, the position of wavelet ridge is searched in $|W_u(a,b)|/\sqrt{a}$.

Assume that the magnitude at the position of wavelet ridge is in the form of

$$|W(a_r(b),b)| = \frac{\sqrt{a_r(b)}}{2} A(b) e^{j\phi(b)} \quad (26)$$

$A(b)$ is the instantaneous amplitude of the signal, and $\phi(b)$ is the instantaneous phase of the signal. $(b, a_r(b))$ is the coordinates of the wavelet ridge in the scalogram.

Then, according to Eq. (26), we can obtain

$$A(b) = \frac{2|W_u(a_r(b),b)|}{\sqrt{a_r(b)}} \quad (27)$$

$$\phi(b) = \text{Ang}[W_u(a_r(b),b)] \quad (28)$$

$\text{Ang}()$ is a function returns the angle of the complex number. The instantaneous angular frequency of the signal is defined as follows

$$\omega(b) = \dot{\phi}(b) = \frac{d \text{Ang}[W_u(a_r(b),b)]}{db} \quad (29)$$

In the next section, we will find the relationship between the coefficients of the nonlinear terms and the three time-frequency variables in (27), (28) and (29).

4. Theoretical analysis of the time-frequency variables

In this section, for the sake of simplicity, we use x instead of x_e . Assume that the weak nonlinearity has the form

$$\varepsilon f(x, \dot{x}) = \sum_{i=1}^p \mu_i |\dot{x}|^i \text{sgn}(\dot{x}) + \sum_{j=1}^q \eta_j |x|^j \text{sgn}(x) \quad (30)$$

where μ_i is the i -th damping coefficient normalized to the mass, and η_j is the j -th stiffness coefficient normalized to the mass. p and q are the orders considered in

the damping and the stiffness system.

The free vibration response $x(t)$ can be represented as

$$x(t) = A(t)\cos(\omega_0 t + \beta(t)) = A(t)\cos(\varphi(t)) \quad (31)$$

where $\varphi(t) = \omega_0 t + \beta(t)$, $A(t)$ and $\varphi(t)$ are the amplitude and phase of $x(t)$. According to the article of Ta and Lardiès (2006), the relationship between the time-frequency variables and the nonlinear parameters is given as follows

$$\begin{aligned} \dot{A}(t) &= -\sum_{i=0}^p \frac{1}{\sqrt{\pi}} \mu_i \omega_n^{i-1} \frac{\Gamma(i/2 + 1)}{\Gamma(i/2 + 3/2)} A^i(t) \\ &= \sum_{i=0}^p c_i A^i(t) \end{aligned} \quad (32)$$

$$\begin{aligned} \omega(t) &= \dot{\varphi}(t) = \omega_0 + \dot{\beta}(t) \\ &= \omega_0 + \frac{\eta_q}{2\omega_0} [1 + (-1)^{q+1}] \left[\frac{\Gamma(q+1)}{2^{q+1}(\Gamma(q/2 + 3/2))^2} \right] A^{q-1}(t) \\ &= \omega_0 + r_q A^{q-1}(t) \end{aligned} \quad (33)$$

where

$$c_i = \frac{1}{\sqrt{\pi}} \mu_i \omega_0^{i-1} \frac{\Gamma(i/2 + 1)}{\Gamma(i/2 + 3/2)} \quad (34)$$

$$r_q = \frac{\eta_q}{2\omega_0} [1 + (-1)^{q+1}] \left[\frac{\Gamma(q+1)}{2^{q+1}(\Gamma(q/2 + 3/2))^2} \right] \quad (35)$$

and $\Gamma(\bullet)$ is the gamma function.

From Ta Minh-Nghi's article, the nonlinearity of the damping only affects the envelope of the signal, while the nonlinearity of the stiffness only relates to phase. This gives us a chance to identify the structure of the model separately. These relationships mentioned above are significant in determining the model and evaluating the parameters in nonlinear models.

The basic steps of identification are summarized as follows:

Step 1: The instantaneous frequency is calculated according to Eq. (29).

Step 2: The instantaneous amplitude is calculated according to Eq. (27).

Step 3: The coefficient μ_i and η_q are obtained according to Eqs. (32)-(35).

5. Experimental study of nonlinear system identification

5.1 The procedure of the experiment

This experiment was divided into four steps. The first step consisted of free vibration tests with different damping cases, i.e., large damping case, medium damping case and

small damping case. To realize free vibrations, a process of push-stable-release of the upper story was adopted.

The second step was parameter identification. Data collected in the first step was used to identify the mathematical model of the structure in different cases.

The third step included the verification of the mathematical model with the identified parameters. A Simulink block diagram was built with the parameters identified in the second part, and the simulation results were compared with the collected data.

In the fourth step, the structure was excited by the El-Centro earthquake. The experimental data was compared with the numerical simulation results to further examine the identified model.

5.2 Nonlinear system identification

5.2.1 Large damping case

The displacement response of the free vibration test is shown in Fig. 5, and its wavelet scalogram of complex Morlet wavelet transform is shown in Fig. 6. According to the method introduced in Section 4, the curve of the instantaneous angular frequency vs. time, the curve of the instantaneous amplitude vs. time and the curve of the instantaneous amplitude vs. its derivative could be obtained and are shown in Figs. 7-9. In Fig. 7, excluding the influence of the edge effect, the slope of the effective middle part of the curve is almost constant. In Fig. 10, a quadratic function $\dot{A}(t) = c_0 + c_1 A(t) + c_2 A^2(t)$ fits the curve well. Therefore, the mathematical model of the structure in the large damping case can be formed as follows

$$\ddot{x} + \omega_0^2 x + \mu_0 \operatorname{sgn}(\dot{x}) + \mu_1 \dot{x} + \mu_2 \dot{x}^2 \operatorname{sgn}(\dot{x}) = 0 \quad (36)$$

And

$$\omega(t) = \omega_0 \quad (37)$$

$$c_0 = \frac{-2\mu_0}{\pi\omega_0} \quad (38)$$

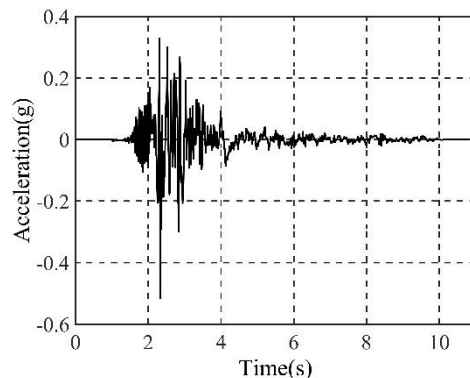


Fig. 4 El-Centro wave

$$c_1 = \frac{-\mu_1}{2} \tag{39}$$

$$c_2 = \frac{-4\mu_2\omega_0}{3\pi} \tag{40}$$

We obtained ω_0 by averaging the angular frequency on the ridge from 1 s to 3 s. Based on the data between 2 s and 5 s from the data in Fig. 9, we calculated coefficients $c_i, (i = 0, 1, 2)$ by the least square method. From Fig. 10, we could see that the identified curve fits well with the experimental data. Then, $\mu_i, (i = 0, 1, 2)$ by Eqs. (38)-(40) was calculated as shown in Table 1.

The mathematical model of the structure with large damping was identified as follows

$$\ddot{x} + 17.79^2 x + 11.08 \text{sgn}(\dot{x}) + 1.01\dot{x} + 0.0032\dot{x}^2 \text{sgn}(\dot{x}) = 0 \tag{41}$$

Table 1 Identified parameters under large damping case

Parameters	ω_0	μ_0	μ_1	μ_2
values	17.79	11.08	1.01	0.0032

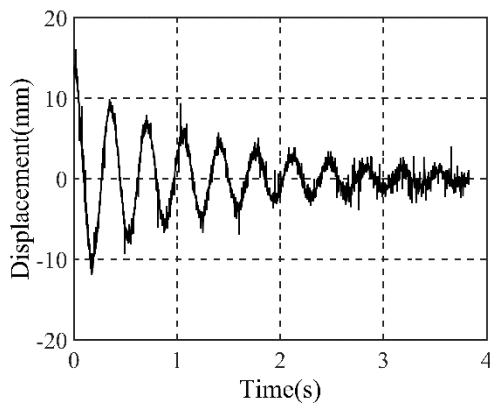


Fig. 5 Displacement response of free vibration under large damping case

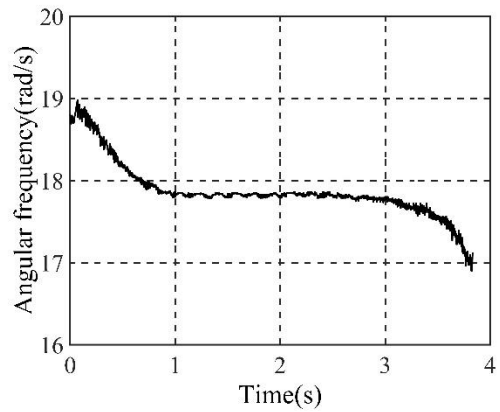


Fig. 7 Instantaneous angular frequency

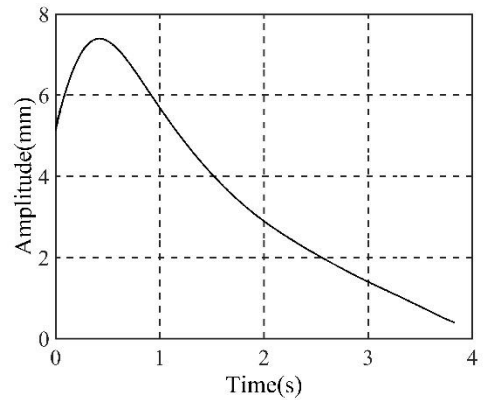


Fig. 8 Instantaneous amplitude

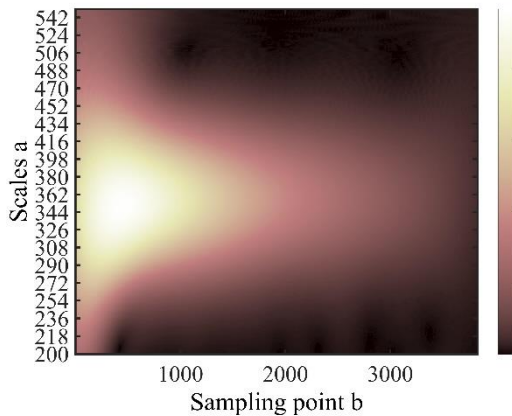


Fig. 6 Wavelet transforms scalogram

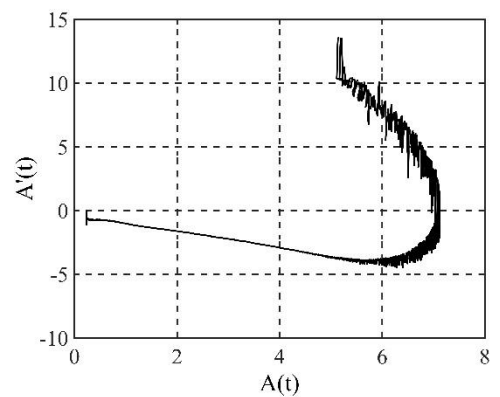


Fig. 9 Instantaneous amplitude vs. its derivative

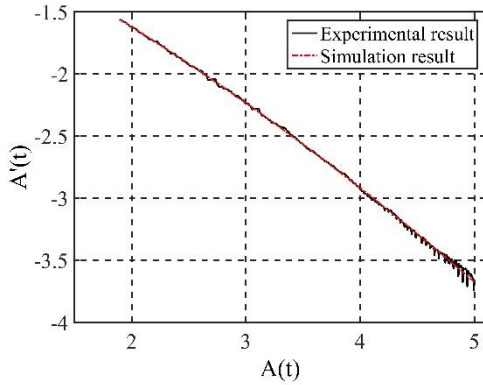


Fig. 10 The fitting results of the experimental data

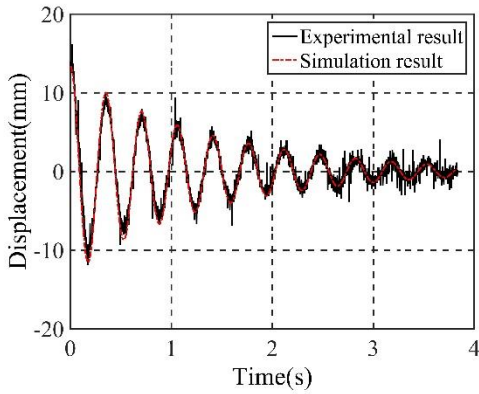


Fig. 11 Comparison of simulation and experimental results of free vibration

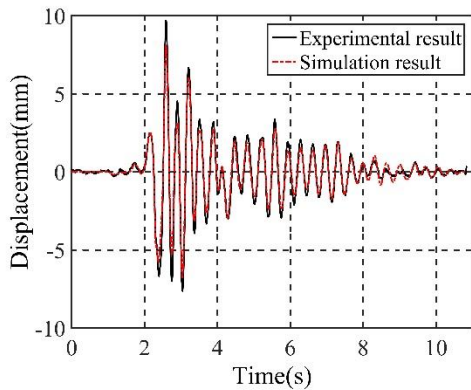


Fig. 12 Comparison of simulation and experimental results under earthquake excitation

Based on the mathematical model in Eq. (41), we built a Simulink model to proceed with the second step. As is shown in Fig. 11, the simulation result was compared with the experimental data.

For further verification, El-Centro earthquake record was exerted to both the SIMULINK model and the experiment model. It is clear in Fig. 12 that the simulation result fits well with the experimental data. The quantitative

comparison of simulation and experimental data will be discussed in Section 5.2.4.

5.2.2 Medium damping case

The analysis procedure of this section is similar to the large damping case. Remove the influence of the edge-effect part, the angular frequency is almost as steady as a constant, as is expressed in Fig. 15. In Fig. 17, the instantaneous amplitude exhibits linear correlation with its derivative. Assume that $\dot{A}(t) = c_0 + c_1 A(t)$, the mathematical model could be written as

$$\ddot{x} + \omega_0^2 x + \mu_0 \text{sgn}(\dot{x}) + \mu_1 \dot{x} = 0 \tag{42}$$

and

$$\omega(t) = \omega_0 \tag{43}$$

$$c_0 = \frac{-2\mu_0}{\pi\omega_0} \tag{44}$$

$$c_1 = \frac{-\mu_1}{2} \tag{45}$$

Similar with the large damping case, the analysis process are exhibited in the Figs. 13-20. The identified parameters of Eq. (42) are listed in Table 2.

Finally, the mathematical model of the structure with the medium damping is

$$\ddot{x} + 17.67^2 x + 3.48 \text{sgn}(\dot{x}) + 1.87 \dot{x} = 0 \tag{46}$$

Table 2 Identified parameters under medium damping case

Parameters	ω_0	μ_0	μ_1
values	17.67	3.48	1.87

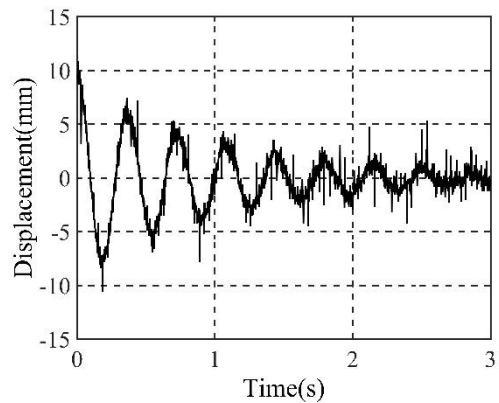


Fig. 13 Displacement response of free vibration under medium damping case

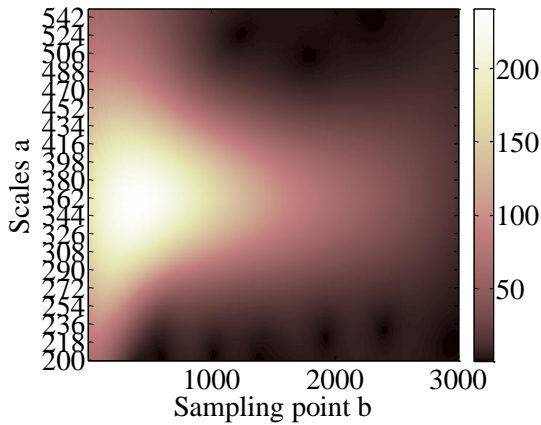


Fig. 14 Wavelet transform scalogram

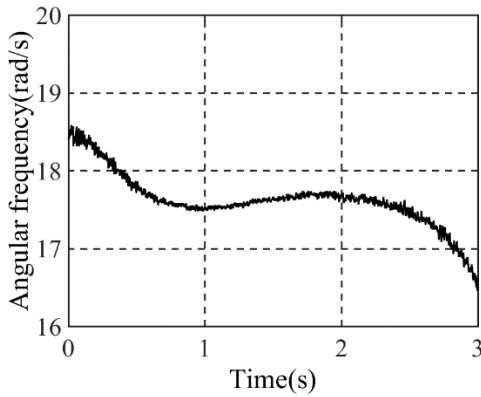


Fig. 15 Instantaneous angular frequency

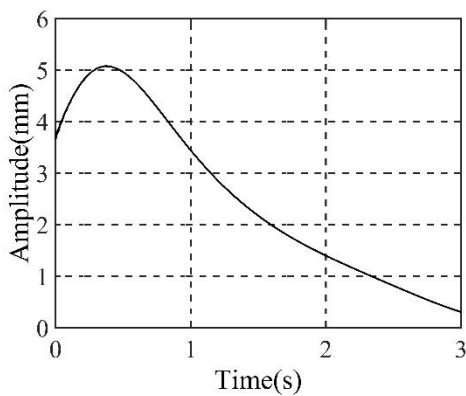


Fig. 16 Instantaneous amplitude

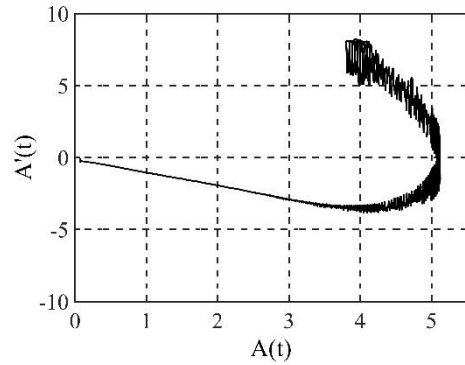


Fig. 17 Instantaneous amplitude vs. its derivative

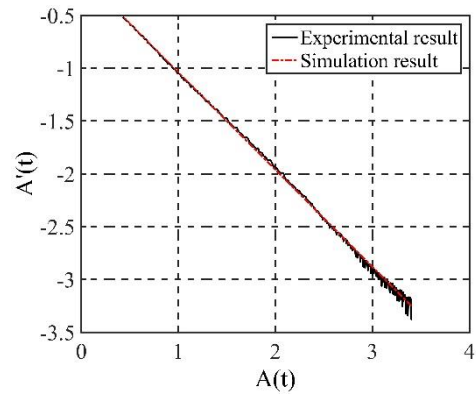


Fig. 18 The fitting results of the experimental data

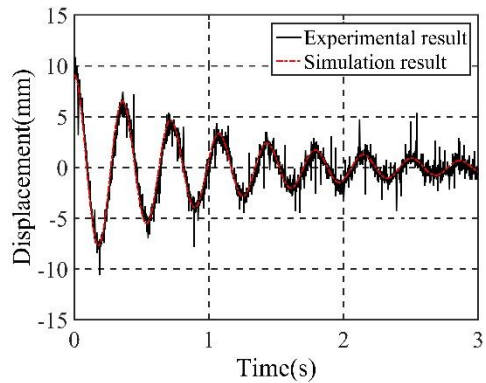


Fig. 19 Comparison of simulation and experimental results of free vibration

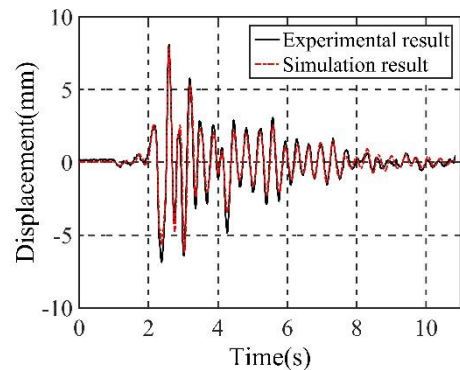


Fig. 20 Comparison of simulation and experimental results under earthquake excitation

Comparison of the simulated result with the experimental data in Figs. 19 and 20 also indicate good match of the identified model and its experimental counterpart.

5.2.3 Small damping case

In this case, although the data shows fluctuate of the the instantaneous angular frequency in Fig. 23, we first suppose it to be constant for the convenience of calculation. From the data trend depicted in Fig. 25, we assumed that $\dot{A}(t) = c_0 + c_1 A(t)$. Then, the mathematical model of the structure was set as

$$\ddot{x} + \omega_0^2 x + \mu_0 \operatorname{sgn}(\dot{x}) + \mu_1 \dot{x} = 0 \tag{47}$$

and

$$\omega(t) = \omega_0 \tag{48}$$

$$c_0 = \frac{-2\mu_0}{\pi\omega_0} \tag{49}$$

$$c_1 = \frac{-\mu_1}{2} \tag{50}$$

The identified parameters are presented in Table 3.

The mathematical model of the structure with small damping is

$$\ddot{x} + 16.86^2 x - 10.80 \operatorname{sgn}(\dot{x}) + 1.97 \dot{x} = 0 \tag{51}$$

The comparison results are demonstrated in Figs. 27 and 28.

The results imply that the assumption of a constant instantaneous angular frequency acquire sufficiently good estimation of the structure.

Table 3 Identified parameters under small damping case

Parameters	ω_0	μ_0	μ_1
values	16.86	-10.80	1.97

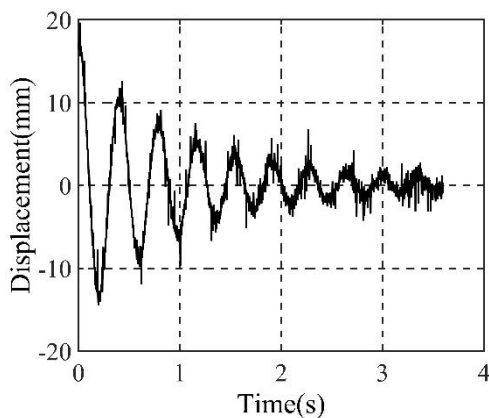


Fig. 21 Displacement response of free vibration under small damping case

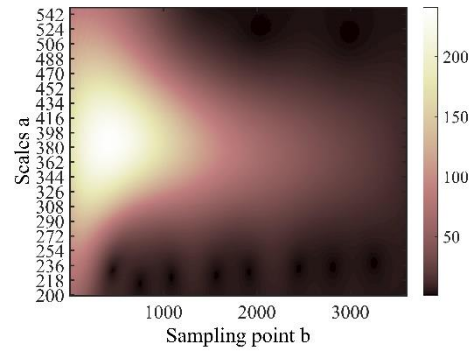


Fig. 22 Wavelet transform scalogram

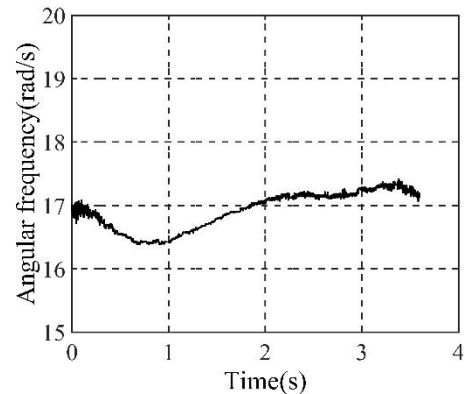


Fig. 23 Instantaneous angular frequency

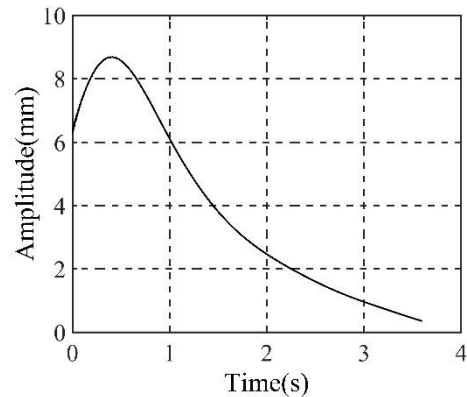


Fig. 24 Instantaneous amplitude

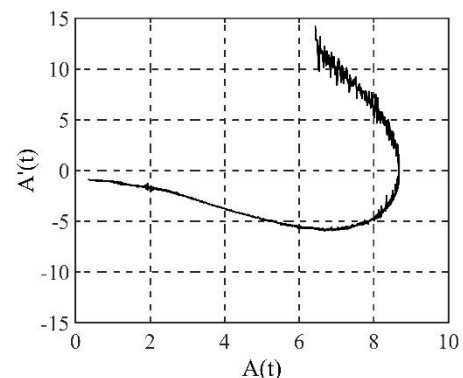


Fig. 25 Instantaneous amplitude vs. its derivative

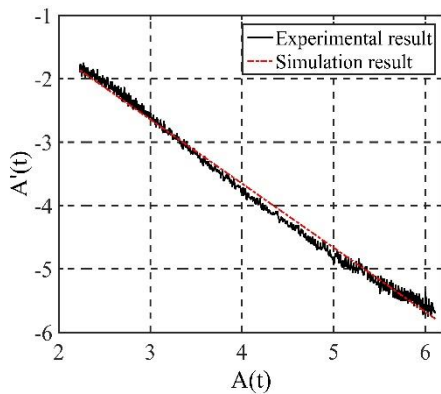


Fig. 26 The fitting results of the experimental data

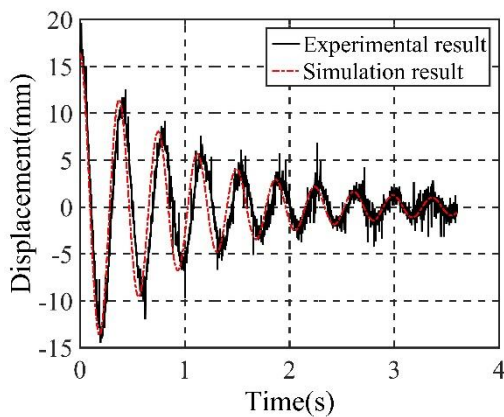


Fig. 27 Comparison of simulation and experimental results of free vibration

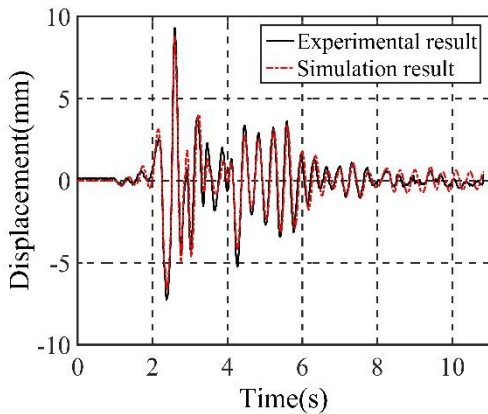


Fig. 28 Comparison of simulation and experimental results under earthquake excitation

5.2.4 Error analysis

The maximum error and standard deviation error of the displacement response between experimental measurement and numerical simulation of the structure under earthquake excitation serve as a criteria to manifest the difference between the mathematical model and experiment model in

different cases. These two criterion are shown in (52) and (53).

$$\text{Maximum error} = \frac{\max(\text{abs}(x_1)) - \max(\text{abs}(x_2))}{\text{abs}(x_1)} \quad (52)$$

$$\text{Standard deviation error} = \frac{\text{std}(x_1) - \text{std}(x_2)}{\text{std}(x_1)} \quad (53)$$

$\text{abs}()$ returns the absolute value of the input variable, $\text{std}()$ returns the standard deviation of the input variable, $\text{max}()$ returns the maximum value of the input variable. x_1 is the displacement responses of the experimental measurement and x_2 is the numerical simulation of the structure under earthquake excitation.

The results in three different cases are provided in Table 4. In this Table, it is apparent that the identified model basically match the experiment model. As the nonlinearity increase with the damping, the error increased with the nonlinearity.

The error might be caused by inaccuracy of the assumed form of the mathematical model, the polynomial model cannot explain every behavior of the tested frame. Though error exists, this method showed good efficiency in recovering the behavior of the test experimental model. This existing problem would be studied in further research.

6. Conclusions

In this paper, a nonlinear experimental model was proposed to imitate nonlinear behavior of one story steel frame under horizontal excitation. The plastic hinge effect was offered by two adjustable viscous dampers. With this experimental model, experiments can be operated repeatedly, and nearly identical vibration records can be reproduced as many as required. With the aforementioned benefits, this experimental model could be used as a benchmark for the verification of nonlinear analysis, control and identification methods.

Table 4 Error analysis under different cases

Large damping	Maximum error (%)	8.77
	Standard deviation error (%)	14.17
Medium damping	Maximum error (%)	8.45
	Standard deviation error (%)	10.79
Small damping	Maximum error (%)	7.09
	Standard deviation error (%)	8.45

A time frequency method based on wavelet transform is introduced to identify the mathematical model of the structure. Three cases under the condition of different damping levels were studied. The model structure and parameters were identified with free vibration data. The simulation result fits well with the observed data. Earthquake excitation tests were conducted to further verify the identified model. The results are compared in Table 4 indicating good performance of the identified model and effectiveness of the identification method.

In the future research, the mathematical model would be improved to better describe the behavior of the physical model and the identification method would be improved to adapt it to large nonlinear cases.

Acknowledgements

This work was supported in part by the National Science Foundation of China under Award No. 51378093, 51678116 and 51678108.

References

- Adams, D.E. and Allemang, R.J. (2000), "A frequency domain method for estimating the parameters of a non-linear structural dynamic model through feedback", *Mech. Syst. Signal Pr.*, **14**(14), 637-656.
- Amari, S.I. (1998), "Neural learning in structured parameter spaces - natural riemannian gradient", *Adv. Neural Inform. Process. Syst.*, 127-133.
- Asgarieh, E., Moaveni, B. and Stavridis, A. (2014), "Nonlinear finite element model updating of an infilled frame based on identified time-varying modal parameters during an earthquake", *J. Sound Vib.*, **333**(23), 6057-6073.
- Aykan, M., and Nevzat Özgüven, H. (2013), "Parametric identification of nonlinearity in structural systems using describing function inversion", *Mech. Syst. Signal Pr.*, **40**, 356-376.
- Dai, Y., Sun, H., Li, H. and Tang, W. (2009). "Identification of weak nonlinearities in damping and stiffness based on wavelet transform", *J. Vib. Shock*, **28**(2), 51-55.
- Delprat, N., Escudie, B., Guillemain, P., Kronlandmartinet, R., Tchamitchian, P. and Torresani, B. (1992). "Asymptotic wavelet and Gabor analysis: Extraction of instantaneous frequencies", *IEEE T Inform. Theory*, **38**(2), 644-664.
- Gere, J.M. and Timoshenko, S.P. (1991), *Mechanics of Materials*, 3rd Ed., *Journal*.
- Haber, R. and Unbehauen, H. (2010), "Structure identification of nonlinear dynamic systems—a survey on input/output approaches", *Automatica*, **26**(4), 651-677.
- Kitada, Y. (1998), "Identification of nonlinear structural dynamic systems using wavelets", *J. Eng. Mech. - ASCE*, **124**, 1059-1066.
- Le, T. and Paultre, P. (2012), "Modal identification based on continuous wavelet transform and ambient excitation tests", *J. Sound Vib*, **331**(9), 2023-2037.
- Ma, F., Ng, C.H. and Ajavakom, N. (2006), "On system identification and response prediction of degrading structures", *Struct. Control Health Monit.*, **13**, 347-364.
- Magnevall, M., Josefsson, A., Ahlin, K. and Broman, G. (2012), "Nonlinear structural identification by the "Reverse Path" spectral method", *J. Sound Vib.*, **331**(4), 938-946.
- Mallat, S. (1999), *A wavelet tour of signal processing, second edition*. Academic Press, San Diego, California, USA.
- Moaveni, B. and Asgarieh, E. (2012), "Deterministic-stochastic subspace identification method for identification of nonlinear structures as time-varying linear systems", *Mech. Syst. Signal Pr.*, **31**, 40-55.
- Noël, J.P. and Kerschen, G. (2013), "Frequency-domain subspace identification for nonlinear mechanical systems", *Mech. Syst. Signal Pr.*, **40**(2), 701-717.
- Ortiz, G.A., Alvarez, D.A. and Bedoya-Ruiz, D. (2013), "Identification of Bouc–Wen type models using multi-objective optimization algorithms", *Comput. Struct.*, **114-115**, 121-132.
- Rice, H.J. and Fitzpatrick, J.A. (1988), "A generalised technique for spectral analysis of non-linear systems", *Mech. Syst. Signal Pr.*, **2**(2), 195-207.
- Shi, Z.Y., Shen, L. and Law, S.S. (2006), "Parameter identification of ITV dynamical system based on wavelet method", *Proceedings of the 4th International Conference on Earthquake Engineering*, Taipei, Taiwan, October.
- Staszewski, W.J. (1998), "Identification of non-linear systems using multi-scale ridges and skeletons of the wavelet transform", *J. Sound Vib.*, **214**(4), 639-658.
- Ta, M. and Lardiès, J. (2006), "Identification of weak nonlinearities on damping and stiffness by the continuous wavelet transform", *J. Sound Vib.*, **293**(1-2), 16-37.
- Wang, C., Ren, W. and Huang, T. (2009), "System identification of a nonlinear structure based on wavelet transformation", *J. Vib. Shock*, **28**(3), 10-13.
- Yan, B.F., Miyamoto, A. and Brühwiler, E. (2006), "Wavelet transform-based modal parameter identification considering uncertainty", *J. Sound Vib.*, **291**, 285-301.
- Zhou, L., Wu, S., Jann, N. and Yang, F.A. (2008). "Experimental study of an adaptive extended kalman filter for structural damage identification", *J. Infrastruct. Syst.*, **14**, 42-51.

BS